Optical and electric characteristics of CuO nanoparticle-doped ZnO thin films using thermionic vacuum arc deposition system

Zehra Nur Ozer[1,*] , Mehmet Ozkan[2], and Suat Pat[3]

[1] *Afyon Vocational School, Afyon Kocatepe University, Afyonkarahisar, Turkey*
[2] *Department of Physics, Afyon Kocatepe University, Afyonkarahisar, Turkey*
[3] *Department of Physics, Faculty of Science, Eskişehir Osmangazi University, 26040 Eskisehir, Turkey*

ABSTRACT

In this study, the thermionic vacuum arc (TVA) method was employed to fabricate thin films of zinc oxide (ZnO) doped with copper oxide nanoparticles (CuONPs). The primary objective was to investigate the influence of the substrate on the characteristics of the CuONPs-doped ZnO thin films. CuONPs were synthesized using both the solution plasma process and the high-voltage liquid plasma generation method, resulting in particle sizes ranging from 20 to 40 nm. The X-ray diffraction (XRD) pattern confirmed the polycrystalline nature of the CuONPs. The prepared CuONPs in powder form were blended with ZnO powder and utilized as an anode material for TVA discharge and coating. The structural, optical, elemental, and topological properties of the resulting thin films were systematically examined. The findings revealed that the deposited thin films exhibited a polycrystalline structure, with transparent and electrically conductive layers. Similar reflection values were observed for films deposited on both glass and indium tin oxide (ITO)-coated glass substrates. Nanostructures on the film surfaces were elucidated through field emission scanning electron microscopy images. The atomic ratios of Cu/Zn were determined as 1/3 and 1/10 for films deposited on uncoated and ITO-coated glass substrates, respectively. The mean grain size of the nanoparticles on the film surface measured approximately 17 nm for films deposited on uncoated glass substrates and 35 nm for those deposited on ITO-coated glass substrates. The film resistance was measured at 20 kΩ, indicating its suitability as a semiconductor. Analysis of the XRD pattern identified peaks corresponding to CuONPs and ZnO in the deposited films, affirming their polycrystalline nature. In conclusion, the deposited thin films exhibit favorable characteristics for semiconductor applications, and the coating method employed proves to be effective in producing high-quality thin films.

Address correspondence to E-mail: zehraerengil@aku.edu.tr

Springer

1 Introduction

Metal oxide semiconductors have gained significant attention in gas sensing applications due to their ease of use, cost-effectiveness, and suitability for detecting and monitoring various gases. Therefore, they are crucial in applications, such as environmental monitoring, industrial safety, and healthcare.

ZnO is a compound semiconductor material with a wide band gap of 3.37 eV and a high binding energy of 60 meV at room temperature. It also exhibits high electron mobility and excellent thermal and mechanical stability. Thanks to these properties, ZnO coatings have become integral components in numerous recent device developments, spanning a wide range of applications, such as solar cells, supercapacitors, light-emitting diodes, ultraviolet photodetectors, functional surface coatings, sensors, and biomedical applications [1, 2]. Recently, studies have focused on the effect of doping metal oxides in improving the electrical, optical, and magnetic properties of ZnO [3–8].

In the literature, several studies have been conducted on composite metal oxide materials [4, 9–13]. These materials have shown dynamic potential, ease of synthesis, versatility in terms of size and shape, and the ability to incorporate various materials. As a result, composite materials are well suited for enhancing the properties of existing materials. CuO is a p-type semiconductor with a band gap of 1.21–1.1 eV. It has various applications, such as superconductors, gas sensors, solar cells, electronics, and semiconductors. The presence of interfacial connections between grains in multi-component semiconductor nanocomposites facilitates efficient charge interaction, allowing for easy modification of the optical and electrical properties of these systems to be easily modified. Among semiconductors with medium or narrow band gaps, CuO possesses advantages, such as chemical stability, the ability to form heterojunctions with ZnO, and a suitable band edge position that can be coupled with ZnO.

In this study, CuO nanoparticles (CuONPs)-doped ZnO thin films were deposited using TVA deposition technology, which is known for producing high-quality and uniformly doped thin films and coatings. The TVA technique provides an opportunity to obtain unique properties or enhance semiconductors [14–19]. Nanoparticles and nanomaterials have changed all the properties of semiconductors or doped semiconductors, exhibiting unique properties compared to bulk materials and undoped semiconductors. Therefore, CuONPs have been selected for doping the ZnO semiconductor. Doped thin films have been analyzed using atomic force microscopy (AFM), field emission scanning electron microscopy (FESEM) with an integrated energy-dispersive X-ray analysis device, and UV–Vis spectrophotometry. These techniques were employed to assess the morphological, optical, structural, and elemental properties of the thin films. Recent literature includes studies on Zn doping or Cu doping CuO or ZnO thin films as mentioned above. To the best of our knowledge, this work represents the first application of the TVA technique in the fabrication of CuO-doped ZnO thin films. In conclusion, a comprehensive investigation has been conducted to explore the optical and electrical properties of these films. It was found that TVA is a good technique for doping nanoparticles, and the samples exhibit semiconductor properties.

2 Experimental

CuONPs have been prepared using the solution plasma process (SPP). After obtaining high-purity CuO particles, they were weighed in appropriate amounts for mixing. CuONPs-doped ZnO thin films are prepared using the TVA technique, while glass and ITO have been used as substrate materials. The chemicals and substrates were purchased from commercial firms. The solvents and chemicals have been purchased from Sigma-Aldrich and Alfa Aesar companies in high purity.

2.1 Preparation of CuO nanoparticles (CuONPs) via solution plasma process (SPP)

SPP represents a distinctive approach in the fabrication of metal oxide nanoparticles [20–22]. The experimental configuration employed for the synthesis of CuO nanoparticles is depicted in Fig. 1. The setup necessitates a bipolar DC power supply featuring a voltage range of 0–4 kV, a frequency span of 1–30 kHz, and a pulse width of 4 μs. Moreover, the distance between the tungsten electrodes has been precisely set to 1 mm, and their insertion into the system has been facilitated through ceramic holders. Throughout the SPP manufacturing procedure, the solution underwent continuous stirring at 400 rpm and was maintained
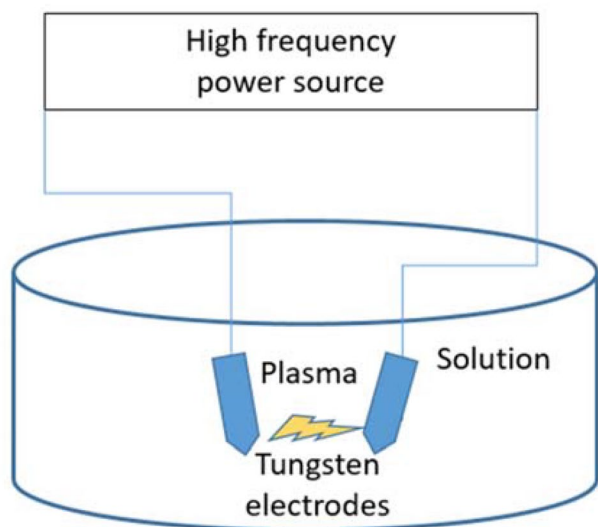
Fig. 1 CuO nanoparticle generation via solution plasma processing (SPP) setup

Fig. 2 XRD pattern of the synthesized CuO nanoparticles (CuONPs) using SPP

Table 1 Parameters of solution plasma processing for CuO nanoparticle generation

Parameter	Value	Unit
Voltage	1500	Volt
Pulse	2.5	µs
Frequency	25	kHz
Distance between electrodes	1	mm
Duration	30	min
pH	4.58 (for $Cu(NO_3)_2$)	

at room temperature using a magnetic stirrer. The detailed process parameters are outlined in Table 1.

To prepare the aqueous solution of $Cu(NO_3)_2$, 10 mL of a 50-mM copper nitrate ($Cu(NO_3)_2$) solution was utilized. The solution was subjected to mixing by applying a voltage of 1.5 kV at a frequency of 25 kHz and a pulse width of 2 µs, facilitated by a magnetic stirrer. A bipolar pulse DC power supply was employed to ensure the continuous generation of plasma within the solution. Subsequently, CuO nanoparticles (NPs) were filtered at room temperature and washed with distilled water.

In Fig. 2, the XRD pattern of CuONPs has been plotted. For the synthesis of CuONPs, the reflection plane peaks at different 2θ values have been obtained. These 2θ values represent the $(\bar{1}10)$, (002), (111), $(\bar{2}02)$, (020), (202), $(1\bar{1}3)$, (311), (113), $(\bar{2}20)$, and (113) crystal planes at 32.49°, 35.49°, 38.96°, 48.73°, 53.62°, 58.33°,
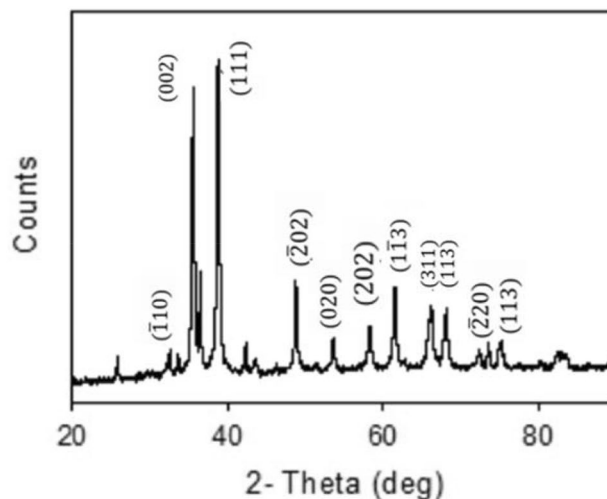
61.62°, 66.29°, 68.19°, 73.58°, and 75.31°, respectively. These results demonstrate a strong correlation with the data card from the international diffraction center (JCPDS-80-1916), confirming the presence of nanoparticles in both monoclinic and polycrystalline structures. According to the obtained XRD result, CuONPs show good crystallinity. The grain size of the obtained CuONPs is about 20–40 nm. The values have been calculated from the XRD pattern using the Scherrer equation [23–27].

2.2 Preparation of CuONPs-doped ZnO thin films by TVA technique

The TVA technique is a method used for depositing thin films and coatings. It operates within a vacuum chamber to ensure high purity and precise control over the properties of the film. In the TVA technique, a low-voltage power source is used to supply energy to a heated cathode filament. This heat causes the cathode filament to emit electrons through a process known as thermionic emission. These emitted electrons are then accelerated by applying a high voltage between the cathode and anode. The electrons are directed toward the anode, where the material to be deposited (often in the form of a pellet) is positioned. When the material reaches a certain vapor pressure, a vacuum arc discharge is initiated between the heated cathode and the anode. During this arc discharge, a significant amount of the evaporated material ionizes, forming plasma.

This plasma contains both neutral atoms and ions of the material. The directed energy of these ions can be controlled, enabling precise manipulation of the film's characteristics [27–34].

TVA is commonly used to produce high-purity and high-quality thin films. This technology is suitable for a wide range of applications, including optoelectronics and coatings in various industries [27–34]. Its operation under high vacuum conditions ensures that the resulting films are free from contamination, making it a valuable technique for both research and industrial applications.

The coating procedure took place inside a vacuum chamber with continuous monitoring of essential factors, such as pressure, current, and voltage. Detailed experimental parameters and their values can be found in Table 2. The substrate holder has been carefully positioned near the anode electrode. Upon applying the appropriate voltage to both the anode and cathode, the pellet inside the crucible undergoes a melting phase, followed by vaporization toward the substrate holder.

2.3 Analysis methods

A Bruker D8 Advance model XRD diffractometer has been used to analyze the microstructural properties of the thin film. CuKa has been mounted onto the device, and XRD analyses have been conducted at room temperature. Powder diffraction technique was used to analyze. The Scherrer equation relates to the full width at half maximum (FWHM) and q values. The equation is given in Eq. 1 [23–27]. The Scherrer equation

Table 2 Experimental deposition parameters were used for the synthesis of CuONPs-doped ZnO thin films on uncoated glass and indium tin oxide-coated glass

Material	CuONPs-doped ZnO (ZnO: 0,07 g, CuO:0,01 g)
Coating pressure	8.10^{-5} torr
Discharge current	$0 \rightarrow 500$ mA
Acceleration voltage	$800 \rightarrow 100$ V
Coating time	75 s
Substrate	Glass and ITO-coated glass
Thickness	320 nm for glass and 82 nm for ITO-coated glass
Roughness	4 nm for glass and 10 nm for ITO-coated glass

provides information about the size of sub-micrometer crystallites in a solid material or thin film. Crystallite sizes (D) are calculated using the following equation.

$$D = \frac{K\lambda}{\beta\cos\theta},$$ (1)

where K is the numeric shape factor and its value can range from 0.62 to 2.08 and for the ZnO material, K is generally taken 0.89. λ represents the X-ray wavelength used, β is the breadth of the full width at half maximum (FWHM), and θ refers to the diffraction angle.

A Hitachi Regulus8230 field emission scanning electron microscopy (FESEM) device with an integrated energy-dispersive X-ray spectrophotometer has been used to analyze the surface properties and chemical compositions of the coated samples. In the FESEM measurement, no coating has been applied to the samples. Additionally, EDX analyses have been used to determine the atomic and weight ratios of the deposited CuONPs-doped ZnO thin films.

The surface morphologies of the samples have also been analyzed using an Ambios Q-scope atomic force microscopy (AFM) device. AFM is a non-contact analysis device with high precision for investigating the properties of nanoscale materials and nanomaterials. The analyses have been applied directly using the wave mode analysis method. AFM analyses were performed at room temperature and a silicon cantilever was used. The scanning frequency was adjusted to 5 Hz, and the scanning area was set to 5 μm × 5 μm. In addition, roughness and surface analyses can be performed using an AFM device and operating software.

To determine the optical constants, transmittance, absorbance, refractive index, and thickness of the coated samples, measurements were taken using a UV–Vis spectrophotometer and a Filmetrics thin film thickness measurement system. As a UV–Vis spectrophotometer, the Unico UV 4802 double-beam spectrophotometer was used to record the obtained spectra in the wavelength range of 200–1100 nm. To determine the band gap and transition type of the deposited films, the optical method has been used. The following equation (Eq. 2) is a well-known equation used to determine the band gap value of a material. The resulting graph should exhibit exponential growth [35–40].

$$(\alpha h\vartheta)^{\mathrm{m}} = \alpha_0(h\vartheta - E_{\mathrm{g}}).$$ (2)

Herein, $h\vartheta$ is the incident photon energy. m is an integer. h is the Planck constant. α_0 is a constant. E_g is the band gap of the semiconductor. m provides key information about the nature of the optical transition [37–39]. The optical transition type defines the following rules [35–40]:

– $m = 2$ for direct allowed transitions.
– $m = \frac{1}{2}$ for direct allowed transitions.
– $m = \frac{2}{3}$ for direct forbidden transitions.
– $m = \frac{1}{3}$ for indirect forbidden transitions.

α is the absorption coefficient of a semiconductor thin film. α can be calculated from Eqs. 3 and 4.

$$\alpha = \frac{1}{t}\ln\ln(T), \tag{3}$$

Or

$$\alpha = 2.303 \times 10^7 (1/A)\left(\text{cm}^{-1}\right), \tag{4}$$

where t represents the thickness of the semiconductor material or the coated film and T represents the transmittance value measured from a UV–Vis spectrophotometer device. The plot of Eq. 2 should be exponential, and the tangent of the exponential graph extends to the x-axis of the band gap graph, which represents the incident photon energy (eV) scale.

Electric measurements were conducted using a Keithley 2450 SMU and a four-point method was employed to determine the resistance of the film.

3 Results and discussion

CuONPs-doped ZnO thin films have been deposited onto uncoated glass and ITO-coated glass using a TVA deposition system. The optical and electrical properties of the deposited thin films have been determined. Additionally, the morphological and structural properties of the produced thin films have been presented. The optical properties of the produced thin films were determined using a UV–Vis spectrophotometer and the Filmetrics F20 thin film thickness measurement system. The measurements were conducted at room temperature, covering a wavelength range of 300–1100 nm. Figure 3a and b presents the transmittance and absorbance curves as a function of the film's wavelength. The spectral analysis of CuONPs-doped ZnO-coated glass revealed distinct optical characteristics across a broad range of wavelengths. The measured data, which includes absorbance and transmittance spectra, demonstrates the intricate interaction of this composite material with incident light. The absorbance spectrum displayed significant peaks at specific wavelengths, indicating the material's ability to absorb light energy. In contrast, the transmittance spectrum exhibited different levels of light transmission across the observed wavelengths. The recorded spectra indicate significant optical activity, primarily concentrated in the ultraviolet (UV) region. Notable peaks have been observed in the absorbance data in this region. This suggests the material's ability to selectively absorb UV radiation, which presents a potential application for UV protection. The transmittance spectrum revealed higher transmission rates within the visible light spectrum, indicating the material's potential to allow visible light to pass through. This characteristic could be valuable for applications that require controlled light transmission, such as in optical filters or photovoltaic devices. Furthermore, the distinct peaks and valleys observed in the spectral data may be attributed to the specific composition and thickness of the CuONPs-doped ZnO coating. The diverse optical behavior across different wavelengths indicates the material's potential for customized performance in various applications. In Fig. 3c, optical band gap plots were provided, and the band gap values were determined to be 2.6 and 3.3 eV for the film deposited onto uncoated and ITO-coated glass samples, respectively. 2.6 eV is related to the CuONPs, and 3.3 eV is related to the ZnO thin films. The band gap value of the ZnO thin film is slightly shifted to a lower value compared to the literature.

In conclusion, the observed optical behavior of the CuONPs-doped ZnO-coated glass presents an intriguing area for further research and development. This offers a pathway for leveraging its unique characteristics in numerous practical applications within the fields of materials science and optics.

The reflectance (R) and refractive index (n) graphs as a function of wavelength are depicted in Fig. 4a and b. The refractive index value obtained for the CuONPs-doped ZnO thin film on ITO-coated glass remains constant across the entire range of measured wavelengths, approximately 2.1 (Fig. 4a). The data consistently shows a refractive index of approximately 1.8 (Fig. 4b), indicating minimal variability over the specified wavelength range. This consistent refractive index suggests that the material has potential
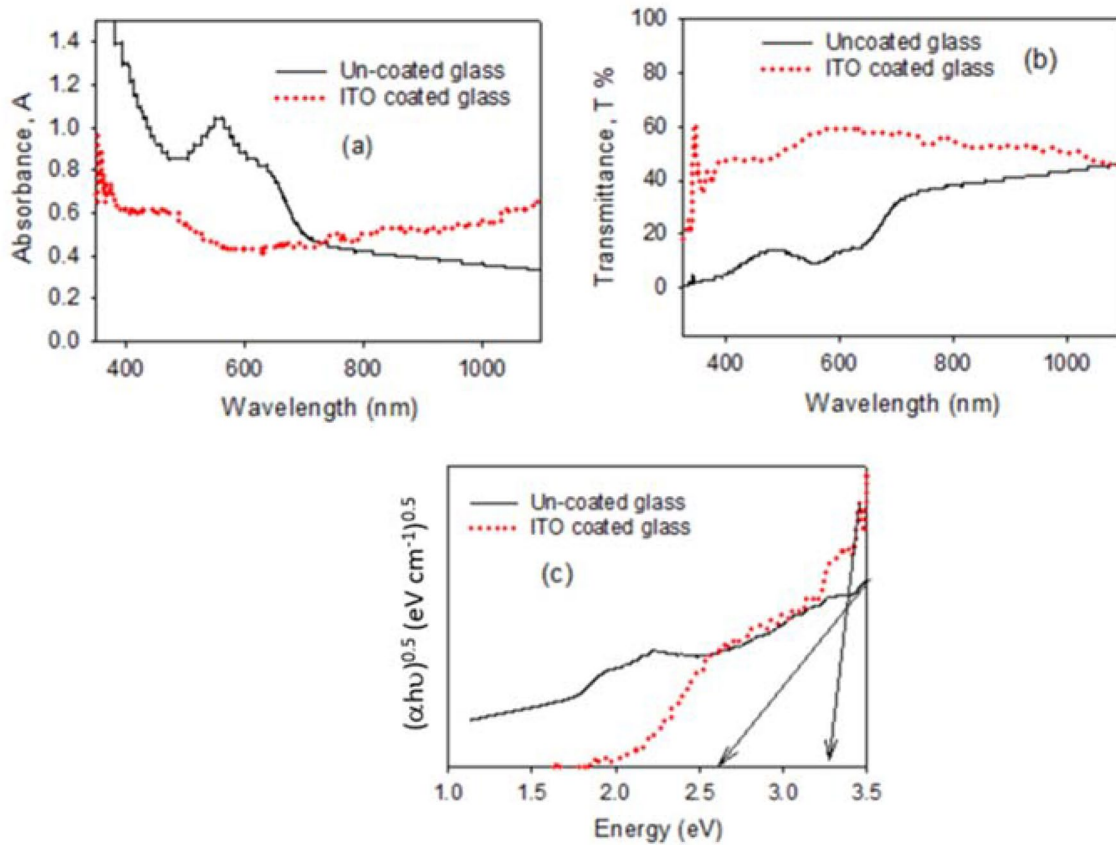
Fig. 3 Absorbance, transmittance, and band gap spectra of CuNPs-doped ZnO thin film onto uncoated glass and indium tin oxide-coated glass substrates
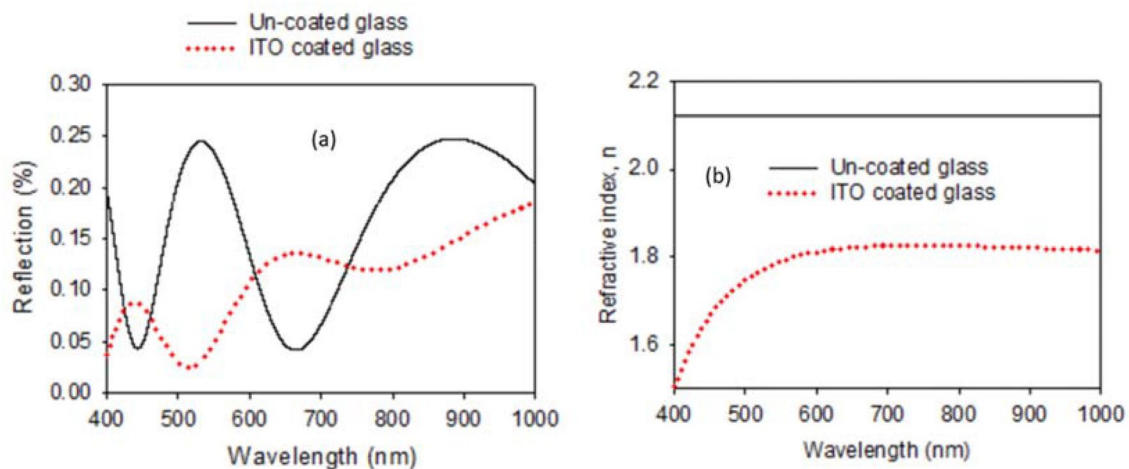

Fig. 4 **a** Reflectance graph and **b** refractive index graphs of CuONPs-doped ZnO thin film onto uncoated glass and indium tin oxide-coated glass substrates

for applications that require uniform optical behavior within the specified range. The reliability of the refractive index across different wavelengths implies a consistent composition and thickness of the coating [41]. This uniformity can be advantageous in various optical applications that require consistent optical

properties within the studied wavelength range. The findings suggest the potential use of CuONPs-doped ZnO-coated ITO in various devices, including anti-reflective coatings, optical filters, and waveguides. This is due to the observed stable refractive index, which offers significant benefits. This constant refractive index emphasizes the material's potential for applications that require predictable and uniform optical characteristics. Moreover, it is recommended to explore the behavior of the material under various environmental conditions in order to gain a comprehensive understanding and enhance its potential applications in the field of optics and photonics. In summary, the uniform and constant refractive index obtained across the spectrum indicates a promising application of CuONPs-doped ZnO-coated ITO in various optical devices. This also emphasizes the stability and reliability of its optical properties within the measured wavelength range. Further studies should explore the behavior of the material in various conditions and its correlation with the properties of the material for optimized applications.

The microstructural properties of the deposited thin films are plotted in the XRD patterns. The XRD pattern in the 2θ range from 10° to 80° is shown in Fig. 5a and b and it belongs to CuONPs-doped ZnO thin films deposited onto uncoated glass and ITO-coated glass substrates, respectively. The XRD pattern of the film deposited onto uncoated glass is similar to amorphous structure, but small peaks are seen in XRD pattern. It must be related with the CuONPs and ZnO, because any material is not used to deposit in the TVA system. The XRD pattern is plotted in Fig. 5a. The XRD pattern

given in Fig. 5b shows the poly crystalline form and it is related with the ITO, CuONPs and ZnO. The pattern are very similar the ZnO's XRD pattern. (100) at 32°, (002) at 35° reflection planes and 2θ values were observed and determined peak and peak locations show good fit with published literature [42]. (111) at 41° and (202) at 53° reflections are related with the CuONPs and these peaks were observed in the XRD pattern of the CuONPs (Fig. 2). According to the Scherrer equation (given in Eq. 1), crystallite size of the film deposited onto uncoated and ITO-coated glass was calculated as approximately 170 and 600 nm, respectively. Substrate materials can change the XRD crystalline structure of the film. Peaks relate with the film deposited onto ITO-coated glass in the XRD pattern. So, XRD patterns are seen different. Uncoated glass has an amorphous structure on the country of ITO-coated glass.

FESEM device was used to determine the surface properties of the CuNPs-doped ZnO thin film onto uncoated and ITO-coated glass substrates. The films were analyzed without any conductive layer coating and they are depicted in Fig. 6a and b, respectively. The film deposited onto uncoated glass has interesting image at the scale of 2 μm. Nano vertical rods are seen in Fig. 6a. Different aggregations were also observed onto surface. These structures are related with the CuONPs because, ZnO thin films do not show the similar structure compared the literature [43–47]. Unlike Fig. 6a, nanorod structures are seen in Fig. 6b in the scale of 2 μm. These structures are obtained and proved by the XRD patterns. For Fig. 6a, XRD patterns show the amorphous structures because nanovertical
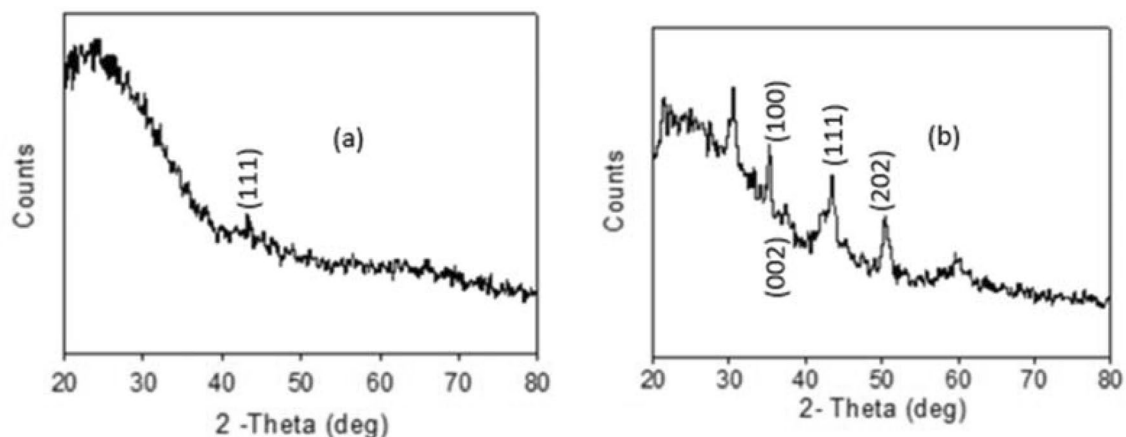

Fig. 5 XRD pattern of CuNPs-doped ZnO thin film onto **a** uncoated glass and **b** indium tin oxide-coated glass substrates

rods are too far too each other. So, X-rays were not consolidate the electromagnetic waves. For Fig. 6b, plane reflections were recorded easily. The surface properties of the film deposited onto ITO-coated substrate are similar to the related literature [48–50]. Additionally, EDX analyses spectra are illustrated in Fig. 6c and d. Cu and Zn atoms were detected in different atomic ratios. The films were coated in same coating route and ratios are different due to substrate effect to coated layers. These ratios are summarized in Table 3. Cu/Zn ratios are determined as to 1/3 and 1/10 for the uncoated glass and ITO-coated glass, respectively.

Another analysis of the deposited thin films is AFM measurements. AFM measurements were done at room temperature and non-contact mode. All AFM images were obtained at 5 μm × 5 μm scale. The AFM images of the film deposited onto uncoated glass and ITO-coated glass are depicted in Fig. 7a and b, respectively. White points are showing the nanovertical rod in Fig. 7a. This was observed in FESEM image (Fig. 6a).

Table 3 EDX analyses results of the CuONPs-doped ZnO thin films deposited onto uncoated glass and indium tin oxide-coated glass

Element	uncoated	ITO coated	Total
Cu	25	9	100
Zn	75	91	100
Cu/Zn	1/3	1/10	

Smaller aggregations are observed in Fig. 7b. Particles size distribution graphs of the deposited thin films are given in Fig. 7c. The mean sizes are 30 and 40 nm for the film deposited onto uncoated and ITO-coated glass substrates, respectively. Additionally, distribution graphs are closely similar to Gauss distribution function and standard deviation is too small. So, particle distributions are homogeny and symmetric on the film surfaces.

To determine the electrical properties of the films, a Keithley sourcemeter unit was used to measure resistance. The resistance of the film has been measured as 20 KΩ. This value is similar to the published values [51, 52]. For a high-quality transparent conductive oxide thin film, the resistance value should be lower than 1000 Ω. According to the results, the deposited sample is a good semiconductor.

Results indicate that TVA is a suitable technology for depositing CuONPs doping onto ZnO thin films, and the deposited thin films exhibit semiconductor properties. CuO doping changes the type of semiconductor and converts it to p-type.

There are recent studies on Zn doping or Cu doping CuO or ZnO thin films in the literature [53–58]. To the best of our knowledge there are limited papers on CuO-doped ZnO thin films produced by different techniques [44, 59] but not using TVA technology. The potential for the occurrence of defects in thin films is increased by the presence of energetic oxygen,
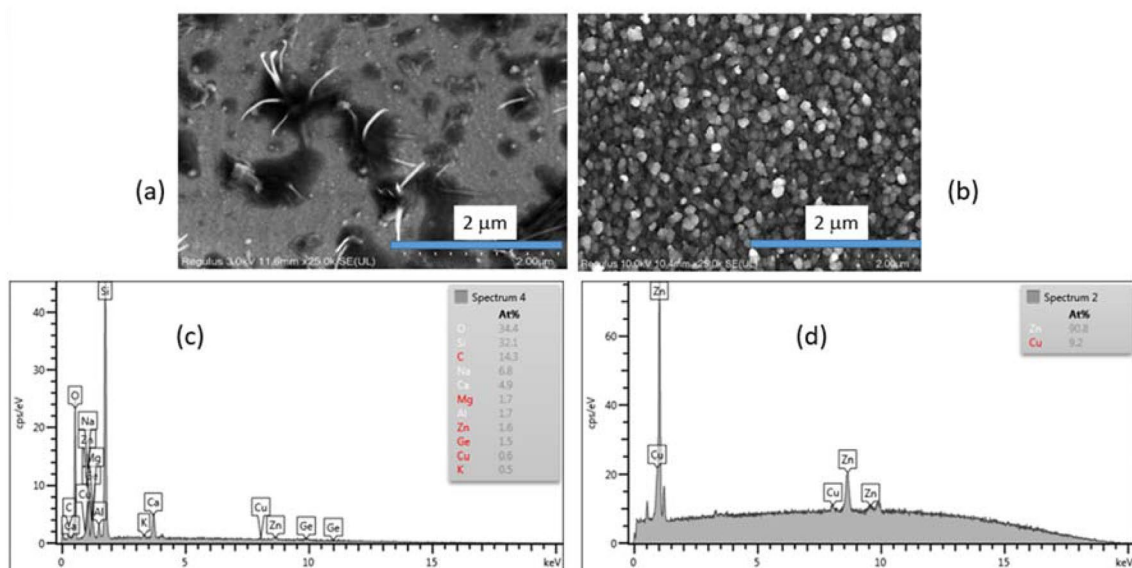

Fig. 6 XRD pattern of CuNPs-doped ZnO thin film onto **a** uncoated glass and **b** Indium tin oxide-coated glass substrates
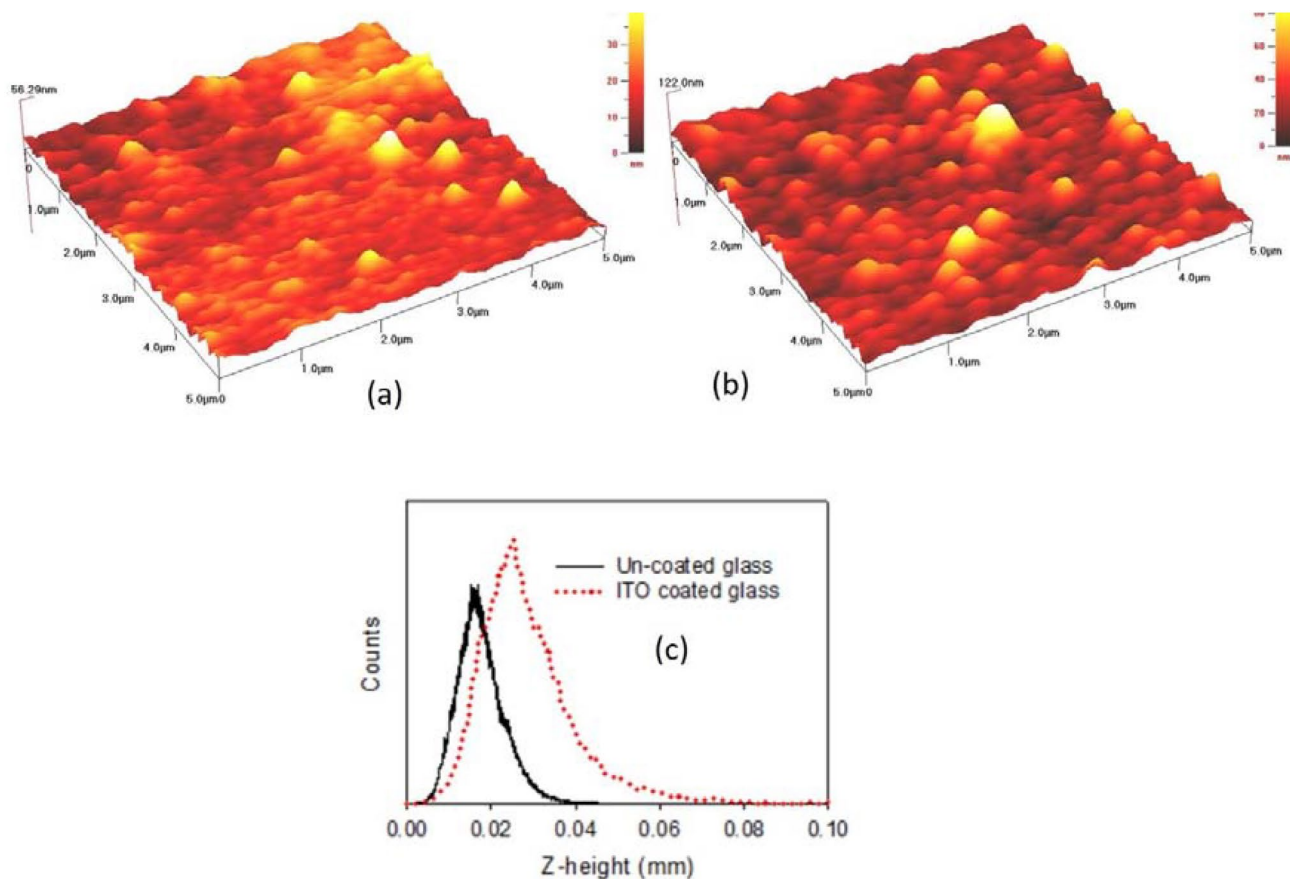
Fig. 7 AFM images of CuNPs-doped ZnO thin film onto **a** uncoated glass and **b** Indium tin oxide-coated glass substrates. **c** Particle size distribution graphs of the deposited thin films

particularly oxygen with high ion energy, which can significantly alter optical flaws. In this context, we are able to decorate energetic oxygen through CuO doping within ZnO. The results in this study showed that TVA can present high-quality CuO-doped ZnO thin films.

4 Conclusion

In this study, CuO nanoparticle (CuONPs)-doped ZnO thin films have been successfully produced using the TVA technique. In literature, various type materials were doped to ZnO thin film, but the properties of the CuONPs-doped ZnO need to be investigated. The effect of nanoparticle material on the optical and electrical properties of the ZnO thin film is the focus of this paper. The structural, optical, microstructural, and topological properties of deposited thin films have been investigated. CuONPs have

been synthesized using SPP. According to the XRD results, CuONPs have been successfully synthesized with a grain size of approximately 20–40 nm calculated using the Scherrer equation. To deposit a thin film, a pressed disk was prepared using CuONPs and ZnO powder. Deposited thin films on uncoated and ITO-coated glass samples are opaque and semi-transparent in the visible region. According to the results of the thin films, the deposited films are opaque and semi-transparent when deposited onto uncoated and ITO-coated glass, respectively. In the XRD pattern of the deposited thin films, the peaks of CuONPs have been identified, indicating the polycrystalline nature of the thin films. The band gap plots of the thin films were determined using the optical method, and the calculated values for CuONPs and ZnO were 2.6 and 3.3 eV, respectively. Finally, the deposited thin films exhibit semiconductor properties, and the TVA deposition technology is an appropriate method for depositing high-quality thin films.

Author contributions

Funding

Data availability

The datasets generated during and/or analyzed during the current study are available from the corresponding author on reasonable request.

Declarations

Conflict of interest The authors declared that there are no conflicts of interest in this work.

Consent for publications During the preparation of this work the author(s) used https://wordvice.ai/ in order to improve the language usage and readability. After using this tool/service, the author(s) reviewed and edited the content as needed and take(s) full responsibility for the content of the publication.

References

1. J. Theerthagiri, S. Salla, R.A. Senthil, P. Nithyadharseni, A. Madankumar, P. Arunachalam, H.S. Kim, Nanotechnology **30**(39), 392001 (2019)
2. H. Safdar, R. Aydın, B. Şahin, Ceram. Int. **48**(18), 26678–26688 (2022)
3. M.H. Bouslama, A. Ouerdane, A. Mokadem, B. Kharroubi, M. Bedrouni, M. Abdelkrim, M.S. Halati, Appl. Surf. Sci. **520**, 146302 (2020)
4. K. Joshi, M. Rawat, S.K. Gautam, R.G. Singh, R.C. Ramola, F. Singh, J. Alloys Compd. **680**, 252–258 (2016)
5. A. Derri, A. Mokadem, A. Ouerdane, K.B. Bensassi, M.H. Bouslama, B. Kharoubi, E. Hameurlaine, Opt. Mater. **145**, 114467 (2023)
6. C. Sudakar, J.S. Thakur, G. Lawes, R. Naik, V.M. Naik, Phys. Rev. B **75**(5), 054423 (2007)
7. G.H. Kim, D.L. Kim, B. Du Ahn, S.Y. Lee, H.J. Kim, Microelectron. J. **40**(2), 272–275 (2009)
8. A. Akkaya, B. Şahin, R. Aydın, H. Çetin, Ayyıldız, J. Mater. Sci. Mater. Electron. **31**(17), 14400–14410 (2020)
9. S.T. Shishiyanu, T.S. Shishiyanu, O.I. Lupan, Sens. Actuators B **107**(1), 379–386 (2005)
10. J.B. Kim, D. Byun, S.Y. Ie, D.H. Park, W.K. Choi, J.W. Choi, B. Angadi, Semicond. Sci. Technol. **23**(9), 095004 (2008)
11. F. Mukhtar, T. Munawar, M.S. Nadeem, M.N. ur Rehman, K. Mahmood, S. Batool, F. Iqbal, Adv. Powder Technol. **32**(10), 3770–3787 (2021)
12. M. Velumani, S.R. Meher, Z.C. Alex, Sens. Actuators B **301**, 127084 (2019)
13. B. Şahin, T. Kaya, Mater. Sci. Semiconduct. Process. **121**, 105428 (2021)
14. S. Pat, R. Mohammadigharehbagh, N.A. Ozgur, B. Oztetik, S. Korkmaz, Phys. B Condens. Matter **640**, 414093 (2022)
15. S. Pat, R. Mohammadigharehbagh, C. Musaoglu, S. Özen, Ş. Korkmaz, Trans. IMF. **99**(6), 286–291 (2021)
16. M. Özgür, S. Pat, R. Mohammadigharehbagh, C. Musaoğlu, U. Demirkol, S. Elmas, Ş. Korkmaz, J. Alloys Compd. **774**, 1017–1023 (2019)
17. S. Elmas, S. Pat, R. Mohammadigharehbagh, C. Musaoğlu, M. Özgür, U. Demirkol, Ş Korkmaz, Phys. B Condens. Matter **557**, 27–33 (2019)

18. C. Musaoğlu, S. Pat, R. Mohammadigharehbagh, S. Özen, Ş. Korkmaz, J. Electron. Mater. **48**, 2272–2277 (2019)

19. M. Ozkan, Z.N. Ozer, *Some Thin-Film Coating Methods, Theory and Research in Engineering II Volume 2*. (330, Gece Publishing, 2020), pp. 119–138. ISBN:978-625-7319-20-1

20. Z.N. Ozer, M. Ozkan, *Solution Plasma Processing and its Applications, Research & Reviews in Engineering - II*. (237, Gece Publishing, 2021), pp. 125–139. ISBN:978-625-8075-45-8

21. B. Oruncak, M. Ozkan, A. Akyuz, Arab. J. Geosci. **13**, 685 (2020)

22. M. Ozkan, B. Oruncak, S. Cevik, El-Cezeri. **7**(2), 543–548 (2020)

23. A.W. Burton, K. Ong, T. Rea, I.Y. Chan, Microporous Mesoporous Mater. **117**(1–2), 75–90 (2009)

24. P.M. Kibasomba, S. Dhlamini, M. Maaza, C.P. Liu, M.M. Rashad, D.A. Rayan, B.W. Mwakikunga, Results Phys. **9**, 628–635 (2018)

25. M. Rabiei, A. Palevicius, A. Monshi, S. Nasiri, A. Vilkauskas, G. Janusas, Nanomaterials. **10**(9), 1627 (2020)

26. E.C. Okpara, O.E. Fayemi, Mater. Res. Express. **6**(10), 105056 (2019)

27. R. Mohammadigharehbagh, S. Özen, H.H. Yudar, S. Pat, Ş. Korkmaz, Mater. Res. Express. **4**(9), 096404A (2017)

28. M.Z. Balbag, S. Pat, J. Plast. Film Sheeting. **27**(3), 209–222 (2011)

29. M.Z. Balbag, S. Pat, M. Ozkan, N. Ekem, G. Musa, Phys. B Condens. Matter **405**(16), 3276–3278 (2010)

30. S. Özen, V. Şenay, S. Pat, Ş Korkmaz, J. Mater. Sci. Mater. Electron. **26**, 5060–5064 (2015)

31. S. Özen, V. Şenay, S. Pat, Ş. Korkmaz, Eur. Phys. J. Plus. **130**, 1–6 (2015)

32. S. Pat, S. Temel, N. Ekem, Ş. Korkmaz, M. Özkan, M.Z. Balbağ, J. Plast. Film Sheeting. **27**(1–2), 127–137 (2011)

33. N.E. Cetin, Ş. Korkmaz, S. Elmas, N. Ekem, S. Pat, M.Z. Balbağ, M. Özmumcu, Mater. Lett. **91**, 175–178 (2013)

34. N. Akkurt, S. Pat, S. Elmas, Ş Korkmaz, J. Mater. Sci. Mater. Electron. **31**, 1293–1301 (2020)

35. Y.E. Firat, A.H.M.E.T. Peksoz, J. Alloys Compd. **727**, 177–184 (2017)

36. S.R. Tokgöz, Y.E. Firat, Z. Safi, A.H.M.E.T. Peksoz, J. Electrochem. Soc. **166**(8), G54 (2019)

37. H.K. Kaplan, S.K. Akay, M. Ahmetoğlu, Appl. Surf. Sci. **601**, 154217 (2022)

38. J.B. Coulter, Phys. Status Solidi (b) **255**(3), 1700393 (2018)

39. P.R. Jubu, F.K. Yam, V.M. Igba, K.P. Beh, J. Solid State Chem. **290**, 121576 (2020)

40. P. Makuła, M. Pacia, W. Macyk, J. Phys. Chem. Lett. **9**(23), 6814–6817 (2018)

41. L.P. Wang, Z.X. Zhang, C.L. Zhang, B.S. Xu, Comput. Mater. Sci. **77**, 281–285 (2013)

42. A.K. Zak, R. Razali, W.A. Majid, M. Darroudi, Int. J. Nanomed. (2011). https://doi.org/10.2147/IJN.S19693

43. S. Das, V.C. Srivastava, Nanotechnol. Rev. **7**(3), 267–282 (2018)

44. K.C. Hsu, T.H. Fang, Y.J. Hsiao, Z.J. Li, J. Alloys Compd. **852**, 157014 (2021)

45. M. Poloju, N. Jayababu, M.R. Reddy, Mater. Sci. Eng. B **227**, 61–67 (2018)

46. J.E. Morales-Mendoza, F. Paraguay-Delgado, Mater. Lett. **291**, 129494 (2021)

47. S. Singhal, J. Kaur, T. Namgyal, R. Sharma, Phys. B Condens. Matter **407**(8), 1223–1226 (2012)

48. N.C.S. Vieira, E.G.R. Fernandes, A.A.A.D. Queiroz, F.E.G. Guimarães, V. Zucolotto, Mater. Res. **16**, 1156–1160 (2013)

49. B. Haspulat-Taymaz, H. Kamış, N. Duyar-Karakuş, Int. J. Sci. Technol. Res. **3**(2), 161–177 (2019)

50. D. Zhang, Y. Tang, Results Phys. **7**, 2874–2877 (2017)

51. S.S. Bharadwaj, B.W. Shivaraj, H.N. Murthy, M. Krishna, M. Ganiger, M. Idris, V.S. Angadi, Mater. Today Proc. **5**(10), 20904–20911 (2018)

52. J. Jońca, K. Fajerwerg, M.L. Kahn, P. Menini, I. Sówka, P. Fau, Sens. Transducers. **259**(5), 99–108 (2022)

53. K. Omri, S. Gouadria, J. Mater. Sci. Mater. Electron. **32**(12), 17021–17031 (2021)

54. Y.H. Navale, S.T. Navale, M.A. Chougule, N.S. Ramgir, V.B. Patil, J. Mater. Sci. Mater. Electron. **32**, 18178–18191 (2021)

55. S.L. Bhise, L.H. Kathwate, G. Umadevi, K.G. Krishna, V.D. Mote, B.N. Dole, J. Mater. Sci. Mater. Electron. **35**(1), 66 (2024)

56. I. Jellal, O. Daoudi, K. Nouneh, M. Boutamart, S. Briche, G. Plantard, J. Naja, J. Mater. Sci. Mater. Electron. **34**(7), 672 (2023)

57. S.D. Lokhande, M.B. Awale, V.D. Mote, J. Mater. Sci. Mater. Electron. **33**(33), 25063–25077 (2022)

58. M. Ozkan, S.S. Erdem, R. Mohammadigharehbagh, S. Pat, J. Mater. Sci. Mater. Electron. **33**(2), 1030–1038 (2022)

59. L. Xu, J. Su, G. Zheng, L. Zhang, Mater. Sci. Eng. B **248**, 114405 (2019)

Springer